Journal of Solid State Chemistry **167,** 59–72 (2002)
doi:10.1006/jssc.2002.9620

Thermal Behavior of Oxometalate (Mo, W)-Intercalated Layered Double Hydroxides: Study of the Grafting Phenomenon

C. Vaysse, L. Guerlou-Demourgues, A. Demourgues, and C. Delmas[1]

Institut de Chimie de la Matière Condensée de Bordeaux, CNRS and Ecole Nationale Supérieure de Chimie et Physique de Bordeaux, 87 Av. Dr A. Schweitzer, 33608 Pessac Cedex, France

Received November 7, 2001; in revised form April 4, 2002; accepted April 19, 2002

The structural evolution of layered double hydroxides (LDHs), containing intercalated free $M_2O_7^{2-}$ oxometalate entities (M = Mo, W), thermally treated up to 800°C, was studied. The intercalated oxometalate anions were shown to be grafted to the slabs at 200°C, on the basis of X-ray diffraction (XRD), which reveals a contraction of the interslab distance, and of EXAFS measurements at the Mo K-edge and the W L(III)-edge, which reveal a change of the local environment of the molybdenum or tungsten atoms. The grafting phenomenon is also confirmed by aging tests in 5 M KOH of the 200°C thermally treated materials, which show that no anionic exchange is possible between the oxometalate and carbonate anions. Geometric considerations, based on the EXAFS results, show that the M_2O_7 entities are grafted to two consecutive slabs, with a local (AB AB) or (AB CA BC) oxygen packing. Nevertheless, no ordered oxygen packing is observed at a large scale. Thermogravimetric studies indicate that the thermal stability is higher for LDHs containing intercalated M_2O_7 entities than for the homologous carbonate-intercalated LDH.

Key Words: **layered double hydroxide; hydrotalcite; oxometalate; thermal behavior; EXAFS; grafting.**

INTRODUCTION

Layered double hydroxides (LDHs) aroused interest in recent years, due to their potential applications as anion exchangers, adsorbents, ionic conductors, precursors of new catalytic materials (1, 2). The structure of these materials consists of brucite-type $[M(OH)_2]$-slabs, in which trivalent cations are substituted for some M divalent cations. This substitution entails a positive charge on the hydroxide layers, which is compensated by interlamellar anions. Water molecules are also present in the interslab space, and contribute to stabilize the structure via a hydrogen bond network involving the anions and the slab hydroxyls. The general formula of the LDHs can be written as follows: $[M^{II}_{1-y} L^{III}_y (OH)_2] X^{n-}_{y/n} [H_2O]_z$, where M^{II} and L^{III} designate the divalent and trivalent cations, and X^{n-} an interlayer anion.

The preparation of such materials can be performed by various methods such as coprecipitation, salt-oxide method, direct anion exchange using a LDH containing intercalated chloride, nitrate or terephthalate anions as precursor, and also reconstruction. In the latter case, the material obtained after calcining a carbonate-inserted LDH is placed in a solution containing the anion to be intercalated, which leads to the reconstruction of the target LDH (3).

An original method involving several "chimie douce" topotactic reaction steps was developed in our lab a few years ago (4, 5). This method, contrary to the usual precipitation methods, consists in decoupling the slab building from the anionic insertion itself. The M^{II}/L^{III} ratio is chosen during the slab building (first step) and controls the amount of inserted anions. A large domain of compositions can, therefore, be obtained by this method, whereas the choice of the slab composition is limited by the intrinsic stability of the final material when using a precipitation method.

Recently, LDHs with the typical formula: $[Ni^{II}_{1-y} Co^{III}_y (OH)_2]^{y+} X^{n-}_{y/n} [H_2O]_z$ ($X^{n-} = Mo_2O_2^{7-}$, $W_2O_7^{2-}$) were obtained in the laboratory, for y values ranging from 0.10 to 0.40 (6). It was shown by several techniques that the intercalated entities are based on two distorted MO_4 tetrahedra (M = Mo, W), linked by a bridging oxygen atom, as in $Cr_2O_7^{2-}$ anions. It should be noticed that possible interesting applications in heterogeneous catalysis are offered to LDHs containing intercalated polyoxometalate anions, either for the freshly prepared materials or after a thermal decomposition (3).

[1]To whom correspondence should be addressed. Fax: +33-5-5684-6634. E-mail address: delmas@icmcb.u-bordeaux.fr.

0022-4596/02 $35.00

The main goal of the present work consists of studying the thermal behavior of these LDHs, intercalated with $Mo_2O_7^{2-}$ and $W_2O_7^{2-}$ species. Similar studies were already reported for CrO_4^{2-} or $Cr_2O_7^{2-}$-intercalated LDHs (7–10). A grafting process of the CrO_4^{2-} and $Cr_2O_7^{2-}$ interlayer species to the slabs was claimed by the authors, the $Cr_2O_7^{2-}$ anions being grafted to the slabs by two oxygen atoms belonging to two CrO_4 tetrahedra. Similar grafting phenomenon was also observed in our lab for LDHs intercalated with $(VO_3)_n^{n-}$ chains (5). A thermal treatment performed on this material indeed showed a decrease of the interslab space, compared to the one observed for the starting LDH, which was attributed to a fragmentation phenomenon of the metavanadate chains into V_2O_7 entities, which were grafted to two adjacent slabs via the two apical oxygen atoms.

Among the obtained LDH series containing intercalated $Mo_2O_7^{2-}$ and $W_2O_7^{2-}$ anions, only the thermal behavior of the materials that exhibit the "$Ni_{0.70}Co_{0.30}$" slab composition will be reported in detail in the present paper, since such composition was shown to lead to a regular stacking of the slabs. For the other compositions, an interstratification phenomenon, resulting from irregular occupancy of the interslab space, appears, which makes the structural characterization, especially the interpretation of the X-ray diffractograms quite complicated as a result of the disorder. The thermal behavior of the materials was investigated by several methods, and particularly X-ray absorption (EXAFS), in order to make precise the structural change of the interlamellar species.

EXPERIMENTAL

As described in a previous paper, the preparation of the LDHs by "chimie douce" consists of three successive steps: (i) preparation of the sodium nickelate, $NaNi_{0.70}Co_{0.30}O_2$, which results in the building of the $Ni_{0.70}Co_{0.30}O_2$ slabs, (ii) oxidation of the sodium nickelate into a γ-oxyhydroxide, (iii) reduction by H_2O_2 of the γ-oxyhydroxide in the presence of molybdate or tungstate anions (6). The final materials will be denoted as $LDH_{0.30}$(Mo) and $LDH_{0.30}$(W) in the following.

The thermogravimetric analysis (TGA), coupled with mass spectrometry, was performed at a rate of $+3$°C/min, from room temperature to 800°C under an oxygen flow.

In order to study accurately the structural and compositional modifications induced by a thermal treatment, the LDHs were treated at 200°C at a rate of $+1$°C/min, under an oxygen flow, for 12 h (the duration of temperature increasing is included in the treatment time). A temperature of 200°C was chosen because it corresponds to the end of the first weight loss on the TGA curve.

The X-ray diffraction (XRD) patterns were recorded on an INEL X-ray diffractometer, equipped with a cobalt anticathode, a forward monochromator and a CPS 120 curved sensitive detector.

Chemical analyses were performed by inductive coupled plasma (ICP) emission spectroscopy for Ni, Co, W and Mo and by elementary organic microanalysis for C and H, at the CNRS facility in Vernaison.

The X-ray absorption measurements were performed on beam line XAS4 at the Laboratoire pour l'Utilisation du Rayonnement Electromagnétique (LURE) in Orsay (France). Molybdenum K-edge (20,000 eV) and tungsten L(III)-edge (10,207 eV) were investigated. A Si(111) monochromator was used for energy selection, leading to a resolution of 2 eV. In any case, a scan of the energy was performed from 100 eV below to 1000 eV above the edges ($\Delta k \approx 16$ Å^{-1}). All the experiments were carried out at room temperature.

RESULTS AND DISCUSSION

The present paper deals with the characterization of the phases that are obtained after a thermal treatment of $LDH_{0.30}$(Mo) and $LDH_{0.30}$(W). Special attention will be devoted to the structural modifications of the interlamellar species and to their way of grafting to the slabs.

X-Ray Diffraction Study

The XRD patterns of the LDHs, obtained before and after a thermal treatment at 200°C, are reported in Fig. 1. In spite of the pronounced turbostratic-like character observed for the $LDH_{0.30}$(Mo) and $LDH_{0.30}$(W) materials, which accounts for the broadening of the (10ℓ) and (11ℓ) lines into two bands and prevents any rigorous indexation, analogies can be made with the XRD pattern of the well-crystallized carbonate-inserted LDH, as reported in detail in a previous paper (6). It can, therefore, be considered that the interslab distance is given by the interreticular distance of the first diffraction line (labelled (00ℓ)), while half the metal–metal distance is given by the position of the (110) line, which corresponds to the lower $2\theta_{Cu}$ values of the (11ℓ) band around 60° ($2\theta_{Cu}$).

After the thermal treatment, the metal–metal distance is unchanged (3.04 Å), showing that the slabs are not affected by the thermal treatment, while the interslab distance decreases significantly from 9.6 Å in the $LDH_{0.30}$(Mo) phase and 9.4 Å in the $LDH_{0.30}$(W) phase to 7.3 Å in the thermally treated materials, which suggests some significant modifications in the interslab space. The distance after the thermal treatment, 7.3 Å, cannot be explained by only water removal out of the interslab space. It is characteristic of the presence of only one oxygen layer in the

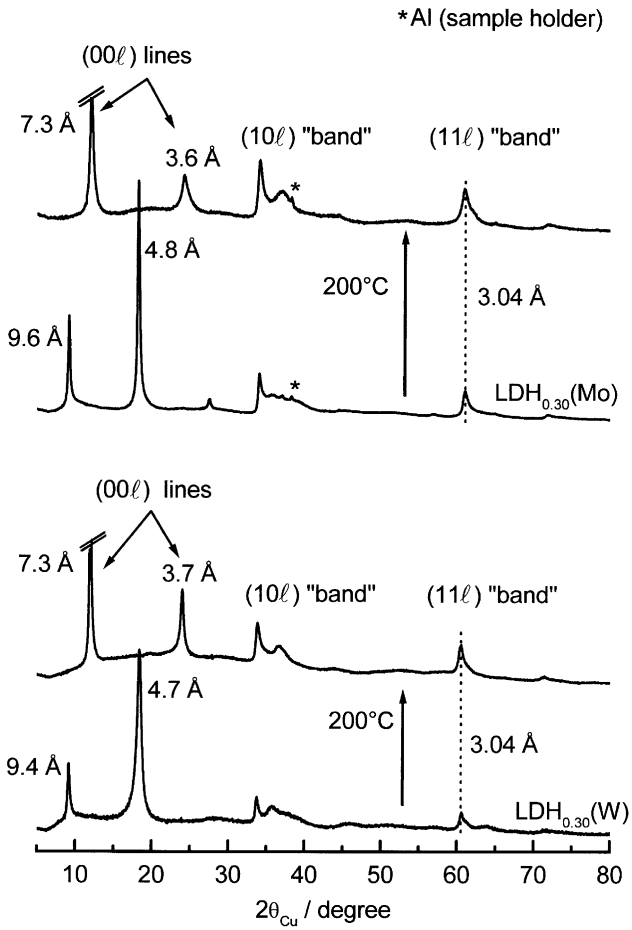

FIG. 1. XRD patterns of the $LDH_{0.30}$(Mo) and the $LDH_{0.30}$(W) phases before and after thermal treatment. The peaks, corresponding to Al, are due to the sample holder.

interlamellar space (5), which is not compatible with free interlamellar $Mo_2O_7^{2-}$ or $W_2O_7^{2-}$ entities within the interslab space. This behavior is attributed to a grafting of the oxoanions to the slabs: two hydroxyl ions of the slabs are replaced by two oxygen ions of the intercalated anion, and strong iono-covalent bonds are created between the anion and the metal cations of the slab.

In order to confirm the grafting hypothesis for the molybdate or tungstate anions after the thermal treatment of the LDHs, a comparative aging test, in 5 M KOH during 2 weeks, was performed for the pristine materials, which contain free intercalated molybdate or tungstate anions and for the materials after the thermal treatment. The XRD patterns of all starting and final materials can be compared in Fig. 2. Starting from the $LDH_{0.30}$(Mo) and the $LDH_{0.30}$(W) phases, the aging in KOH leads to a decrease of the interslab distance from 9.4–9.6 to 7.6–7.7 Å, the final XRD pattern being typical of a carbonate-inserted LDH. This means that, in both cases, an anionic exchange occurs between the oxoanions and the carbonate anions, leading to a $LDH_{0.30}(CO_3)$ phase. This exchange was fully confirmed by infrared spectroscopy. This result can be explained by the anionic exchange properties of LDHs and by the fact that the carbonate anions exhibit a higher affinity for the LDH matrix than all other anions (11). On the contrary, in the case of the thermally treated LDHs, the XRD patterns after the aging test are identical to those of the starting thermally treated LDHs. Such behavior shows that the oxometalate species cannot be exchanged by the carbonate anions and confirms the grafting, after the thermal treatment, of the oxoanions to the slab via strong iono-covalent bonds.

The evolution of the relative intensity of the first two (00ℓ) diffraction peaks, observed during the thermal treatment, will be commented in the General Discussion section.

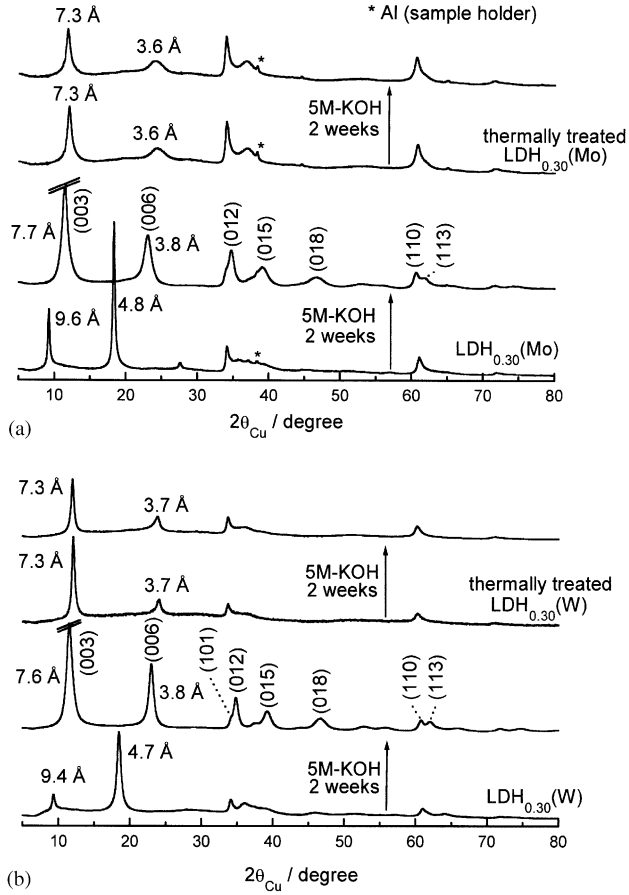

FIG. 2. Evolution of the XRD patterns after the aging in 5 M KOH during 2 weeks of (a) the $LDH_{0.30}$(Mo) and (b) the $LDH_{0.30}$(W) phases before and after the thermal treatment. The peaks, corresponding to Al, are due to the sample holder.

TABLE 1
Values of the A/(Ni + Co) Molar Ratios for Various A Elements in the $LDH_{0.30}$(Mo) and the $LDH_{0.30}$(W) Phases before and after Thermal Treatment

	A	Ni	Co	Mo	C	H
$LDH_{0.30}$(Mo)	Weight %	26.03	10.93	18.10	0.32	2.18
	A/(Ni + Co)	0.71	0.29	0.30	0.04	3.47
$LDH_{0.30}$(Mo), treated at 200°C	Weight %	31.25	13.13	21.74	0.33	1.35
	A/(Ni + Co)	0.71	0.29	0.30	0.04	1.79
$LDH_{0.30}$(W)	Weight %	23.90	9.02	26.75	0.66	2.00
	A/(Ni + Co)	0.72	0.28	0.26	0.10	3.57
$LDH_{0.30}$(W), treated at 200°C	Weight %	26.02	10.08	29.34	0.50	1.21
	A/(Ni + Co)	0.72	0.28	0.26	0.07	1.97

Elemental Chemical Analysis

The weight percentages of nickel, cobalt, oxometalate (Mo, W), carbon and hydrogen in the materials, obtained before and after the thermal treatment, are given in Table 1. As presented in a previous paper (6), the two formulae of the pristine materials are

$$Ni_{0.71}Co_{0.29}(OH)_2(Mo_2O_7)_{0.15}(H_2O)_{0.74}(CO_3)_{0.04(adsorbed)}$$

and

$$Ni_{0.72}Co_{0.28}(OH)_2(W_2O_7)_{0.13}$$
$$(CH_3COO)_{0.02}(H_2O)_{0.71}(CH_3COO)_{0.03(adsorbed)}.$$

As expected, in both systems, the Mo/(Ni + Co) (or W/(Ni + Co)) molar ratio is the same in the pristine LDH phase and in the material that is obtained after the thermal treatment. Besides, an increase of the Ni, Co and Mo or W weight percents is observed after the thermal treatment, while the H weight percent decreases. As it will be shown later by other investigation techniques, this tendency can be explained by the removal of intercalated water and by the beginning of the slab dehydroxylation, due to the grafting of the inserted anions to the slabs.

An IR study was also performed on the thermally treated materials, in comparison with the pristine ones, and no significant change was observed. In order to complete the XRD and the IR studies, which are not sufficient to conclude precisely on the structural modifications of the interlamellar oxomolybdate and oxotungstate species, the materials that were obtained after thermal treatment at 200°C of $LDH_{0.30}$(Mo) and $LDH_{0.30}$(W) were characterized by EXAFS at the Mo K-edge and W L(III)-edge, respectively.

EXAFS Study

Normalized EXAFS data, $k^3\chi(k)$, were obtained by using DARESBURY software; the corresponding Fourier transforms were analyzed using the EXCURV programs. All EXAFS refinements were performed by considering in a first step the metal ions surrounded by a first oxygen shell, and the subsequent shells were gradually added. Except for very special cases, all the coordination numbers were fixed at given values, and the distances, the energy shift and the Debye–Waller factors were refined.

Mo K-Edge. The EXAFS signal and the associated Fourier transform, corresponding to the materials obtained after the thermal treatment, are presented in Figs. 3a and 3b. The Fourier transform that was obtained for the starting $LDH_{0.30}$(Mo) phase (6) is also given in Fig. 3c for comparison. Various parameter values obtained for the thermally treated material and for the pristine material, are summarized in Table 2. In both materials, the refinement leads to two shells, relative to oxygen first and second neighbors, and one shell corresponding to molybdenum neighbors. For the thermally treated material, the first shell is constituted of four oxygen atoms at 1.74 Å, with a small Debye–Waller factor, $2\sigma^2 = 0.006$ Å^2, which shows the existence of a regular tetrahedral oxygen environment for molybdenum. The experimental distance is consistent with the Mo–O distance in a regular MoO_4 tetrahedron, reported in the literature (12). In the case of the pristine $LDH_{0.30}$(Mo) material, the first coordination shell was shown to be constituted of a distorted oxygen tetrahedron, as reported in Table 2 (6). The thermal treatment leads to a more regular tetrahedral environment.

Examination of the Fourier transforms in Figs. 3b and 3c shows that the contribution of the second shell seems to be smaller in the case of thermally treated material. Nevertheless, intensity of the Fourier transform for the thermally treated material is twice that observed for the pristine material, so that the contribution of the second shell can be taken into account.

In order to refine the subsequent shells of the thermally treated material, molybdenum was, in a first step, considered as surrounded by molybdenum neighbors, in

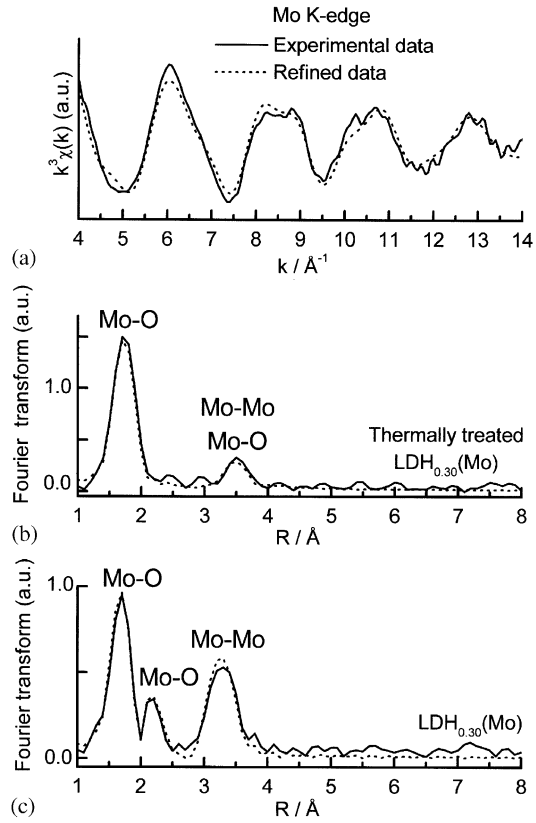

FIG. 3. (a) Mo K-edge EXAFS spectrum and (b) its Fourier transform for the $LDH_{0.30}$(Mo) phase after thermal treatment, in comparison with (c) the Fourier transform for the pristine $LDH_{0.30}$(Mo) phase.

addition to the four oxygen atoms of the first shell at 1.74 Å.The calculation converged in this hypothesis, to one molybdenum neighbor, located at 3.59 Å from molybdenum. The fit was acceptable, but it was significantly improved by considering the presence of an additional sphere, which turned out to be constituted of six oxygen atoms at 3.41 Å. These oxygen atoms may belong to water molecules (improbable after thermal treatment), to surrounding oxomolybdate entities or to the metal oxide slabs. Their location will be addressed in the General Discussion section. It should be noticed that a refinement of the data in the absence of any molybdenum neighbor, i.e., by considering only oxygen neighbors for the second shell, in addition to the four oxygen atoms of the first shell, was also attempted and led to worse results. This behavior confirms the presence of one molybdenum neighbor in the vicinity of the MoO_4 tetrahedron.

The 3.59 Å Mo–Mo distance requires that the MoO_4 tetrahedra share one oxygen atom. If the two MoO_4 tetrahedra were isolated, the Mo–Mo distance would be significantly larger. Therefore, one can assume that $Mo_2O_7^{2-}$ anions are preserved during the grafting to the hydroxide slabs. The Mo–Mo distance that is obtained for the thermally treated material (3.59 Å) is longer than in the starting $LDH_{0.30}$(Mo) phase (3.25 Å); in that case, the Mo–O–Mo angle of the $Mo_2O_7^{2-}$ entities was found close to 115° (6). An opening of this angle explains this difference in size. Besides, the Debye–Waller factor is higher for the material after the thermal treatment ($2\sigma^2 = 0.012$ Å^2) than for the starting one ($2\sigma^2 = 0.005$ Å^2). This behavior is not really understood at this time.

It should be noted that the 2.23 Å Mo–O distance, which was present for the pristine material and attributed to the surrounding interlamellar water molecules (6), has disappeared in the thermally treated material, in agreement with the removal of interlamellar water.

TABLE 2

Parameters Obtained after Refinement of the EXAFS Data at the Mo *K*-Edge for Thermally Treated $LDH_{0.30}$(Mo) and for the Starting Material

Material	Shell	CN	R(Å)	$2\sigma^2$(Å^2)
Thermally treated $LDH_{0.30}$(Mo)	Mo–O	4.0	1.74(1)	0.006(1)
	Mo–O	6.0	3.41(2)	0.017(1)
	Mo–Mo	1.0	3.59(2)	0.012(1)
$LDH_{0.30}$(Mo) (6)	Mo–O	3.0	1.72(1)	0.007(1)
	Mo–O	1.0	1.93(1)	0.008(1)
	Mo–O	2.0	2.23(1)	0.012(1)
	Mo–Mo	1.0	3.25(2)	0.0050(6)

W L(III)-Edge. The EXAFS oscillations at the W L(III)-edge and the corresponding Fourier transform obtained for the thermally treated material are shown in Fig. 4. The data obtained for the starting material are also given for comparison. The Fourier transform obtained for the thermally treated material shows two shells, which exhibit strong similarities with those found in the case of the homologous $LDH_{0.30}$(Mo) phase. The parameters resulting from the modelization are summarized in Table 3. The first shell around tungsten atoms is composed of four oxygen atoms, located at 1.76 Å ($2\sigma^2 = 0.008$ Å^2), which is in complete agreement with the distance given in the literature for tungsten in a regular tetrahedral environment (12).

The refinement of the second shell was not very easy as a result of the poor quality of the EXAFS data. Nevertheless, it seems that the second shell is constituted of oxygen atoms, located at 3.46 Å. Contrary to the case of pristine $LDH_{0.30}$(W), the refinement did not allow to give prominence to the existence of tungsten neighbors for tungsten, whereas the refinement, in the case of the thermally treated molybdenum homologous material,

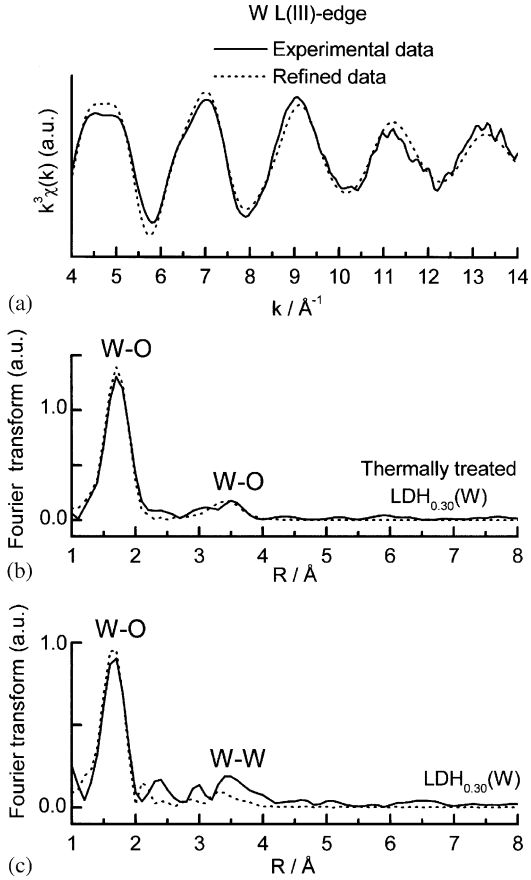

FIG. 4. (a) W L(III)-edge EXAFS spectrum and (b) its Fourier transform for the $LDH_{0.30}(W)$ phase after thermal treatment, in comparison with (c) the Fourier transform for the pristine $LDH_{0.30}(W)$ phase.

showed the presence of one molybdenum neighbor at 3.59 Å.

The position of the M_2O_7 entities (M = Mo, W) within the interslab space will be further discussed in the General Discussion section.

Thermal Stability and Grafting

Thermogravimetric analysis (TGA) coupled with mass spectroscopy. The TGA weight loss curves, as well as the analysis results of the evolved decomposition products by mass spectrometry, are given in Figs. 5 and 6 for $LDH_{0.30}(Mo)$ and $LDH_{0.30}(W)$, respectively.

The thermal decomposition of LDHs has extensively been studied. It is generally agreed that these materials tend to decompose in two distinct steps (13–15): (i) loss of adsorbed and intercalated water molecules, (ii) dehydroxylation of the slabs, destruction of the lamellar structure and formation of mixed metal oxides.

In the case of the $LDH_{0.30}(Mo)$ phase (Fig. 5), the derivative curve obtained from the weight loss curve shows three peaks, corresponding to the three distinct phenomena.

The first stage of weight loss, which ranges from room temperature to 225°C, corresponds to the loss of the whole intercalated water. Nevertheless, the strong decrease above 200°C of the interslab distance from 9.6 to 7.3 Å, previously reported, gives prominence of the grafting of the Mo_2O_7 entities to the slabs. Therefore, this weight loss corresponds to the removal of adsorbed and intercalated water, as it was already observed in the LDHs (13–15), and to the grafting of the $Mo_2O_7^{2-}$ species to the slabs. Two hydroxyl groups of the slab are replaced by two oxygen atoms of the anions, leading to a "chemical" formula, which can be written with "free" OH^- anions in the interslab space:

$$Ni_{0.71}Co_{0.29}(OH)_{1.70}(Mo_2O_7)_{0.15}(OH)_{0.30}.$$

This formula agrees with a loss of 0.74 water molecule observed in the TGA experiment. The loss of interslab water, deduced from the TGA measurements, is confirmed by the presence at 140°C, on the mass spectrometry diagram, of ionic currents corresponding to H_2O^+ and OH^+ ionic species. The above formula has to be compared to the chemical analysis results obtained for the thermally treated material (at 200°C) (Table 1), which show that the H/(Ni + Co) molar ratio = 1.79 versus 2.00 in the above "chemical" formula, deduced from the TGA curve. This means that some "free" OH groups were already lost during the 12-h thermal treatment at 200°C.

The second stage of weight loss, which occurs between 225 and 292°C, may correspond to the reaction of the "free" OH^- groups with the $Mo_2O_7^{2-}$ anions, leading to "isolated" MoO_4^{2-} anions, grafted to the slabs, following the reaction:

$$Mo_2O_7^{2-} + 2\,OH^- \rightarrow 2MoO_4^{2-} + H_2O.$$

The water loss is also detected by mass spectrometry, which shows both H_2O^+ and OH^+ weak ionic currents. The existence of separated MoO_4 entities was not unambiguously proved at this time. Nevertheless, it is supported by a slight variation of the interslab distance in the range 260–300°C, as shown in the following section. EXAFS

TABLE 3
Parameters Obtained after Refinement of the EXAFS Data at the WL(III)-Edge for Thermally Treated $LDH_{0.30}(W)$ and for the Starting Material

Material	Shell	CN	R(Å)	$2\sigma^2$(Å^2)
Thermally treated $LDH_{0.30}(W)$	W–O	4.0	1.76(1)	0.008(1)
	W–O	6.0	3.46(2)	0.027(1)
$LDH_{0.30}(W)$ (6)	W–O	3.0	1.74(1)	0.007(1)
	W–O	1.0	1.95(1)	0.006(1)
	W–W	1.0	3.20(2)	0.019(1)

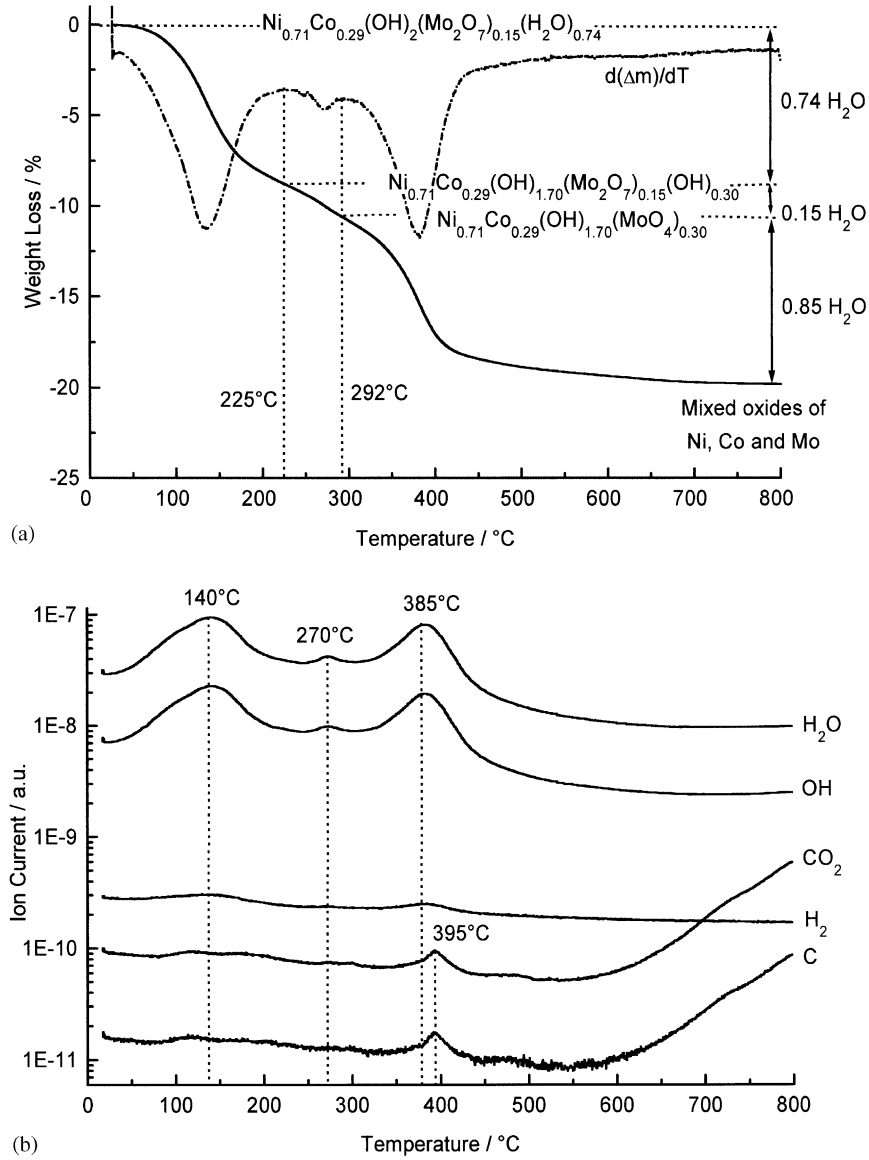

FIG. 5. (a) TGA curve of $LDH_{0.30}(Mo)$ and (b) curve of the mass spectrometry coupled with TGA.

measurements of the material treated at 300°C are planned in order to further investigate the evolution of the interlamellar species. Assuming the existence of MoO_4 motifs, the following "chemical" formula could be proposed for the resulting material:

$$Ni_{0.71}Co_{0.29}(OH)_{1.70}(MoO_4)_{0.30}.$$

This formula also agrees with a loss of 0.15 water molecule observed in the second step of the TGA experiment.

Between 292 and 450°C, the weight loss corresponds to the end of dehydroxylation and to the destruction of the slabs. This result is confirmed by the presence of ionic currents, corresponding to H_2O^+, OH^+, CO_2^+ and C^+ ionic species at 385 and 395°C. The very less carbon amount that is detected may be due to a very small pollution of our material by carbon species during the reduction step or during the analysis experiment. Beyond 450°C, a re-organization of the metal oxides occurs, in order to obtain mixed nickel, cobalt and molybdenum oxides, which were identified by XRD.

In the case of the $LDH_{0.30}(W)$ phase (Fig. 6), only two peaks are present on the derivative curve obtained from the TGA weight loss curve.

The first stage of weight loss seems to be more diffuse than in the case of $LDH_{0.30}(Mo)$ and gathers the first two weight loss steps observed for $LDH_{0.30}(Mo)$. This

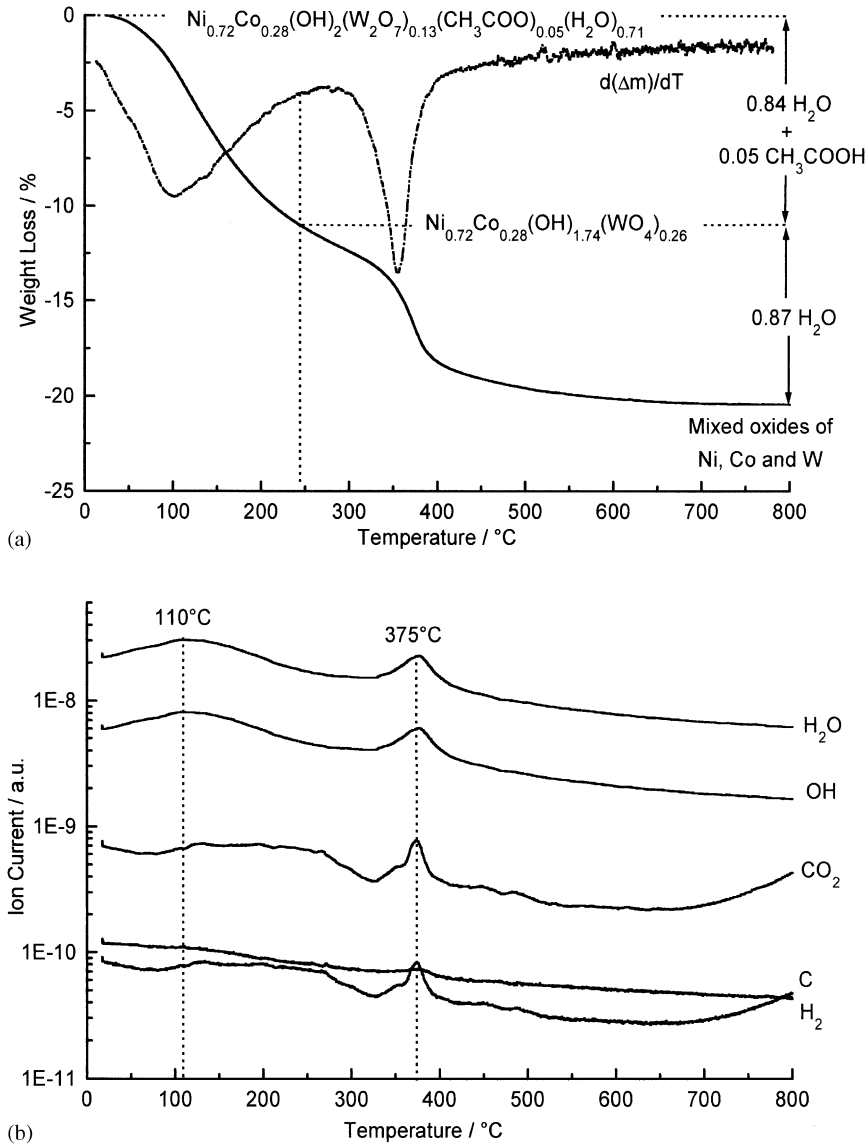

FIG. 6. (a) TGA curve of $LDH_{0.30}(W)$ and (b) curve of the mass spectrometry coupled with TGA.

difference in behavior is certainly due to the presence of the acetate anions, cointercalated in the interslab space during the reduction step to $LDH_{0.30}(W)$ (6). As a consequence, a difference in the strength of hydrogen bonds between the anions, the water molecules and the hydroxyl groups of the slabs occurs, modifying the thermal decomposition process. As suggested by the mass spectrometry results, which show H_2O^+ and OH^+ ionic currents in a large temperature range around 110°C, this first stage of weight loss corresponds to the loss of intercalated water, to the beginning of dehydroxylation and to the fragmentation/grafting of the tungstate species. Moreover, small CO_2^+ and C^+ ionic current peaks are observed; they must correspond to the departure of some acetate anions. Similar to the behavior of the $LDH_{0.30}(Mo)$ material, the following formula can be established on the basis of the weight loss of the TGA curve, $Ni_{0.72}Co_{0.28}(OH)_{1.74}(WO_4)_{0.26}$. It should be noted that, for the $LDH_{0.30}(W)$ phase treated for 12 h at 200°C, the H amount, obtained by the chemical analysis, was slightly higher than that shown in the previous formula, and a small C amount was detected. This can be explained by the fact that, at 200°C, all the acetate anions were not completely removed out of the interslab space.

The second weight loss corresponds to the end of dehydroxylation, to the removal of the remaining acetate ions and to the destruction of the slabs, as revealed by mass spectrometry, which shows H_2O^+, CO_2^+ and C^+ ionic current peaks at 375°C. The final material, characterised by

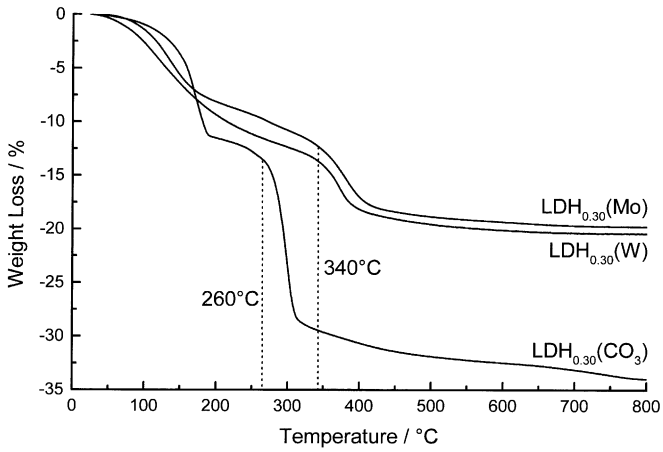

FIG. 7. Comparison of TGA curves of $LDH_{0.30}$(Mo), $LDH_{0.30}$(W) and $LDH_{0.30}(CO_3)$.

XRD, is composed of mixed nickel, cobalt and tungsten oxides.

In conclusion, the $LDH_{0.30}$(Mo) and $LDH_{0.30}$(W) phases exhibit similar thermal behaviors, especially a higher thermal stability in comparison with the $LDH_{0.30}(CO_3)$ phase (typically 80°C more) (Fig. 7). Such behavior was already observed in our lab for LDHs intercalated with $(VO_3)_n^{n-}$ chains (5). It has been proved that a thermal treatment induces a fragmentation phenomenon of the metavanadate chains into V_2O_7 entities, which were grafted to two adjacent slabs. The vanadate-intercalated LDHs are thus thermally stable up to 300°C. This higher stability of oxometalate-intercalated LDHs can be explained by the presence of the oxoanions in the interslab space, which create large pillars between two slabs by through grafting. These pillars support the layered structure, and leads to a better thermal stability of the material, as already observed by Besse *et al.* for dichromate-intercalated LDHs (9, 10). The behavior of carbonate-inserted LDHs during thermal treatment was unclear; therefore, this study was also performed. The results are presented elsewhere (16).

XRD Patterns of $LDH_{0.30}$(Mo) and $LDH_{0.30}$(W) Heated at Different Temperatures. The thermal stability of $LDH_{0.30}$(Mo) and $LDH_{0.30}$(W) was studied by XRD (Fig. 8). The materials were calcined at each chosen temperature during 12 h under an oxygen flow. A similar behavior is observed for both $LDH_{0.30}$(Mo) and $LDH_{0.30}$(W). In the 200–300°C range, no real change occurs in the materials, except for the decrease in intensity of the peak at 3.7 Å, compared to the intensity of the peak at 7.3 Å.This decrease in intensity can be explained by a modification in the arrangement of the interslab species, and by the removal of some OH groups, still present in the interslab space, as it has been seen in the previous part. Moreover, the interslab distance of the lamellar phase is slightly decreased in the 260–300°C temperature range, which could be related to the fragmentation of the M_2O_7 entities to MO_4 ones, suggested by the TGA results. The lamellar structure is maintained until 280–300°C. At 300°C, a partial destruction of the slabs occurs in some domains, as shown by the appearance of the peaks belonging to the NiO phase. Above 300°C, the lamellar structure collapses, and mixed oxides are formed. These results are in agreement with the TGA measurements coupled with mass spectrometry, presented in the previous section; nevertheless, the decomposition temperatures are higher in the TGA measurements, due to the relation between the kinetics effects and temperature rate.

General Discussion

During the thermal treatment at 200°C, the whole results, described before, suggest a grafting of the

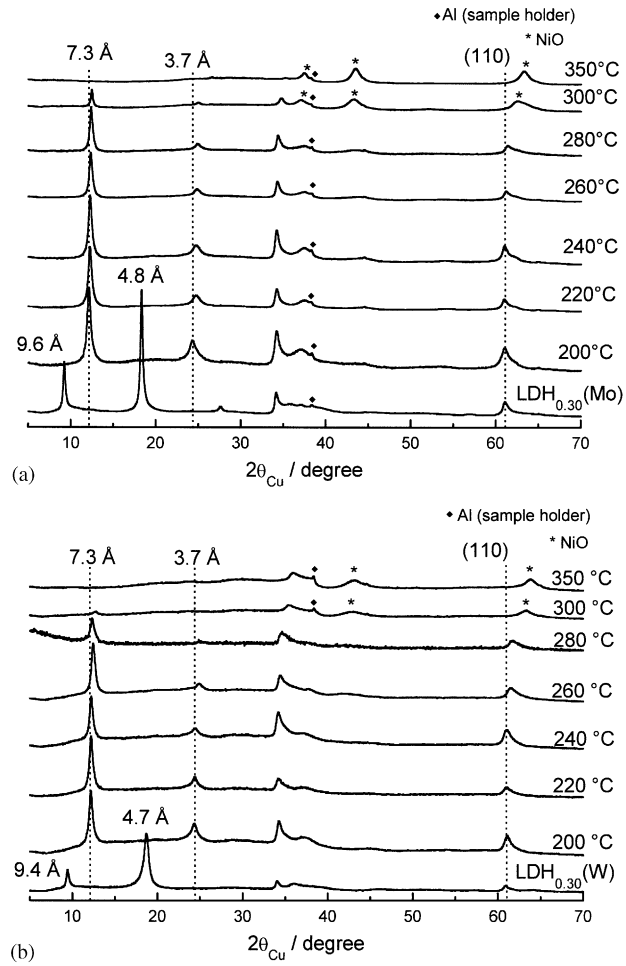

FIG. 8. X-ray diffraction patterns of (a) the $LDH_{0.30}$(Mo) and (b) the $LDH_{0.30}$(W) phases versus temperature. The peaks, corresponding to Al, are due to the sample holder.

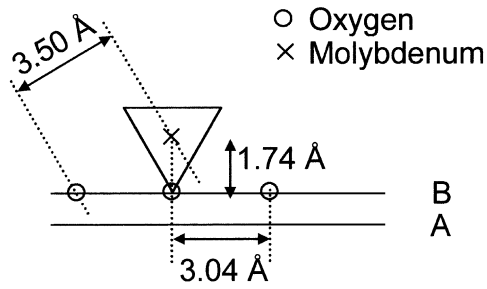

FIG. 9. Schematic representation of one tetrahedron, grafting to the slab. The different O–O and Mo–O distances are reported.

$M_2O_7^{2-}$ entities (M = Mo, W) to the slabs, via the creation of two iono-covalent bonds between two oxygen atoms of the $M_2O_7^{2-}$ anion and two cations of the slabs. From a general point of view, the layered structure can be described from a packing of triangular lattices (A, B, C positions). In each sheet, the unit interatomic distance is equal to 3.04 Å ($a_{hex.}$ parameter). If only one tetrahedron is considered, calculation shows that the six oxygen atoms of the slab are located at a distance of 3.50 Å from the molybdenum atom. This distance was calculated on the basis of the $a_{hex.}$ parameter (3.04 Å, which is the slab metal–metal distance) and of the $Mo–O_{apical}$ distance (1.74 Å), deduced from EXAFS (Fig. 9). This is in full agreement with the EXAFS study, which has shown the existence of a six-oxygen shell, surrounding molybdenum, with a Mo–O distance of 3.41 Å.

The relative positions of the two tetrahedra in the $Mo_2O_7^{2-}$ entities can be discussed, in relation with the various oxygen packing of the hydroxide slabs. The value of the interslab distance shows that one oxygen layer is intercalated between the (Ni, Co)$(OH)_2$ slabs; therefore, one triangular face of the tetrahedra must be in the center of the interslab space (or in its vicinity). Several grafting hypotheses have to be considered. The two tetrahedra can be grafted: (a) to the same slab (Fig. 10a), or to two adjacent slabs. In this case, three different oxygen packing (of the (Ni, Co)$(OH)_2$ slabs) must be considered: (b) AB BC CA (Fig. 10b), (c) AB AB (Fig. 10c), (d) AB CA BC (Fig. 10d). Unfortunately, the XRD lines were too broad to allow an accurate indexation of the XRD patterns, which could confirm the above-mentioned stacking hypotheses. Therefore, only the EXAFS data can be considered in this discussion.

In order to discuss the various structures of the $Mo_2O_7^{2-}$ entities and their various orientations, one has to consider the matching between the interatomic distances and the oxygen packing:

- In hypothesis (a), the grafted molybdenum atoms hang from the oxygen atoms of the slabs, and occupy the same position as the apical oxygen atoms, in a plane that is

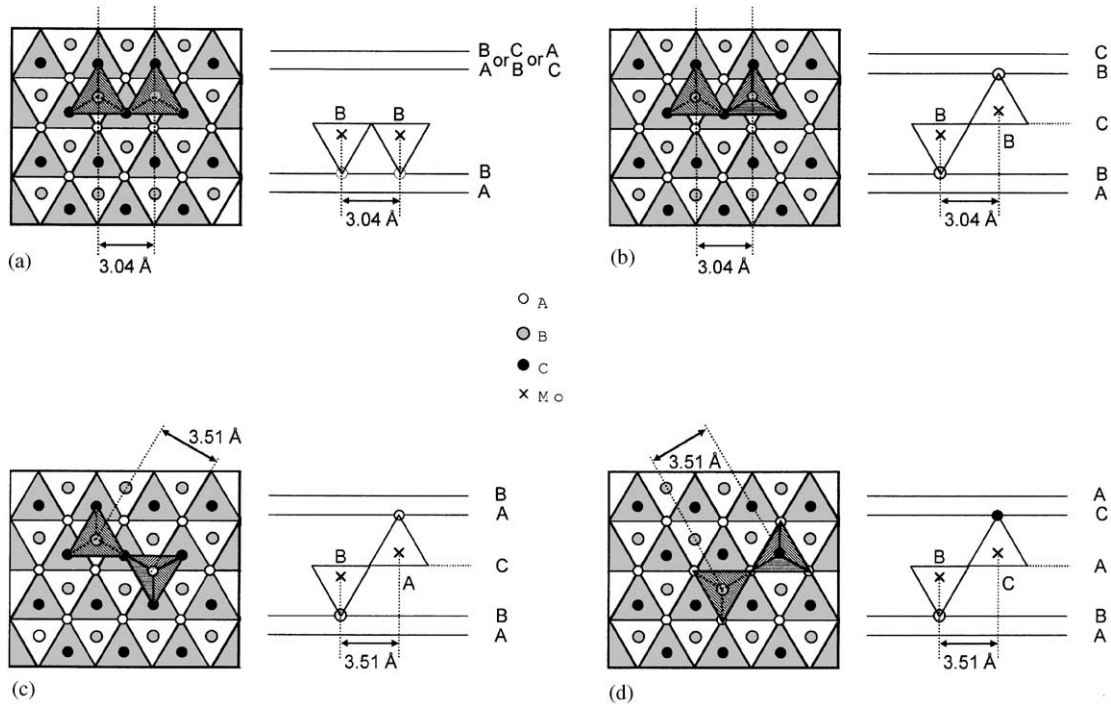

FIG. 10. Grafting scheme of the M_2O_7 entities: (a) to the same slab, and to two adjacent slabs with an (b) (AB BC CA), (c) (AB AB), or (d) (AB CA BC) oxygen packing. Only the (AB) slab and one M_2O_7 entity are represented.

parallel to the slab, so that they must be separated by similar distances as for oxygen atoms, i.e., 3.04 Å for the shortest distance. This distance is not compatible with the one obtained by EXAFS (3.59 Å).

- In hypothesis (b), the oxygen atoms of the slabs exhibit an (AB BC CA) packing (Fig. 10b), so that the oxygen planes surrounding the interslab space are superimposed. Since the apical Mo–O distance is 1.74 Å, the distance between the molybdenum atom and the faces of the tetrahedron is 0.58 Å (if one assumes an ideal tetrahedron). All these results lead to a Mo–Mo distance of 3.25 Å, which is not in good agreement with the 3.59 Å Mo–Mo distance obtained by EXAFS.

- In hypotheses (c) and (d) (Figs. 10c and 10d), the calculated Mo–Mo distances will be identical. The distance between the projected positions of the oxygen atoms in the slab plane is 3.51 Å. This leads to a 3.69 Å Mo–Mo distance in the interslab space, which is in quite good accordance with the distance resulting from EXAFS (3.59 Å).

It should be noted that these Mo–Mo distances were calculated with one triangular face of the MoO_4 tetrahedra in the center of the interslab space. Nevertheless, these tetrahedron faces are probably not parallel to the slabs, so that an angle must exist between them and the centre plane of the interslab space. This behavior induces a larger

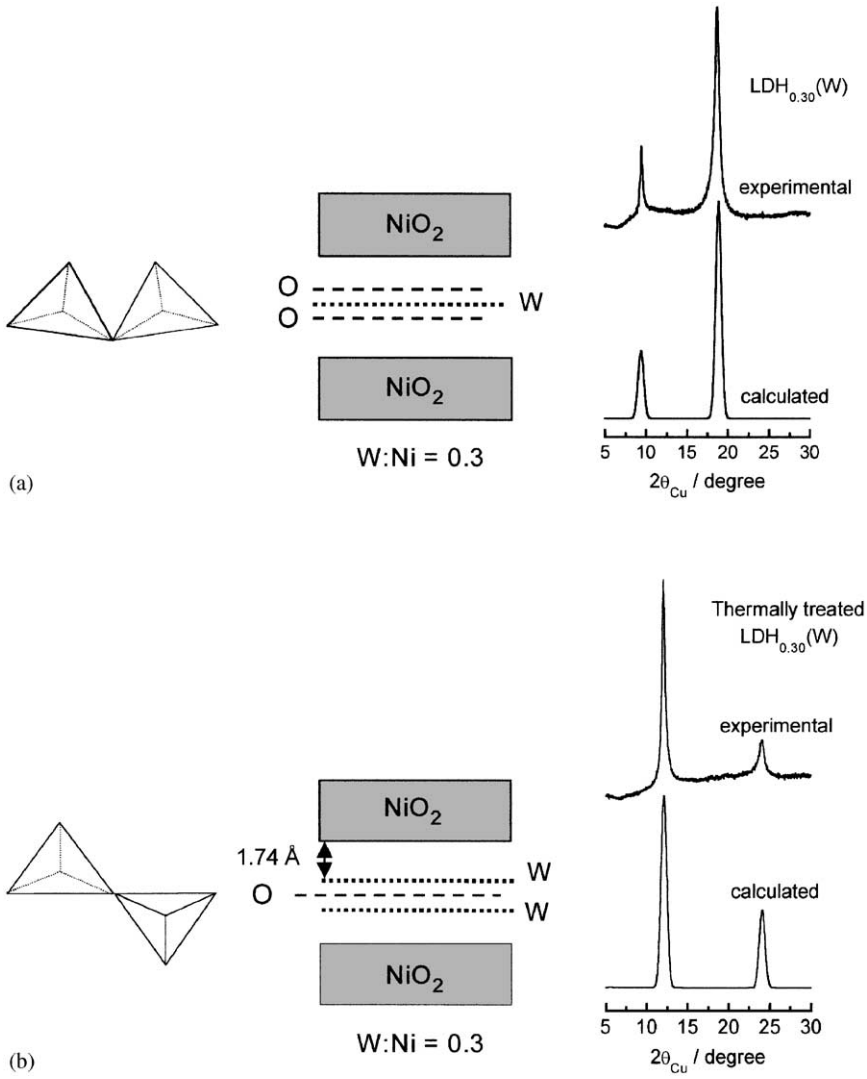

FIG. 11. Comparison between the experimental and calculated XRD patterns of (a) $LDH_{0.30}(W)$ and (b) thermally treated $LDH_{0.30}(W)$. For $LDH_{0.30}(W)$, the WO_2 slab, inserted between the NiO_2 slabs, consists of three successive layers (O, W, O). For the thermally treated $LDH_{0.30}(W)$ phase, two W slabs and one oxygen slab are inserted between the NiO_2 slabs, with W:Ni and $W:O_{interslab}$ ratios equal to 0.30 and 0.40, respectively.

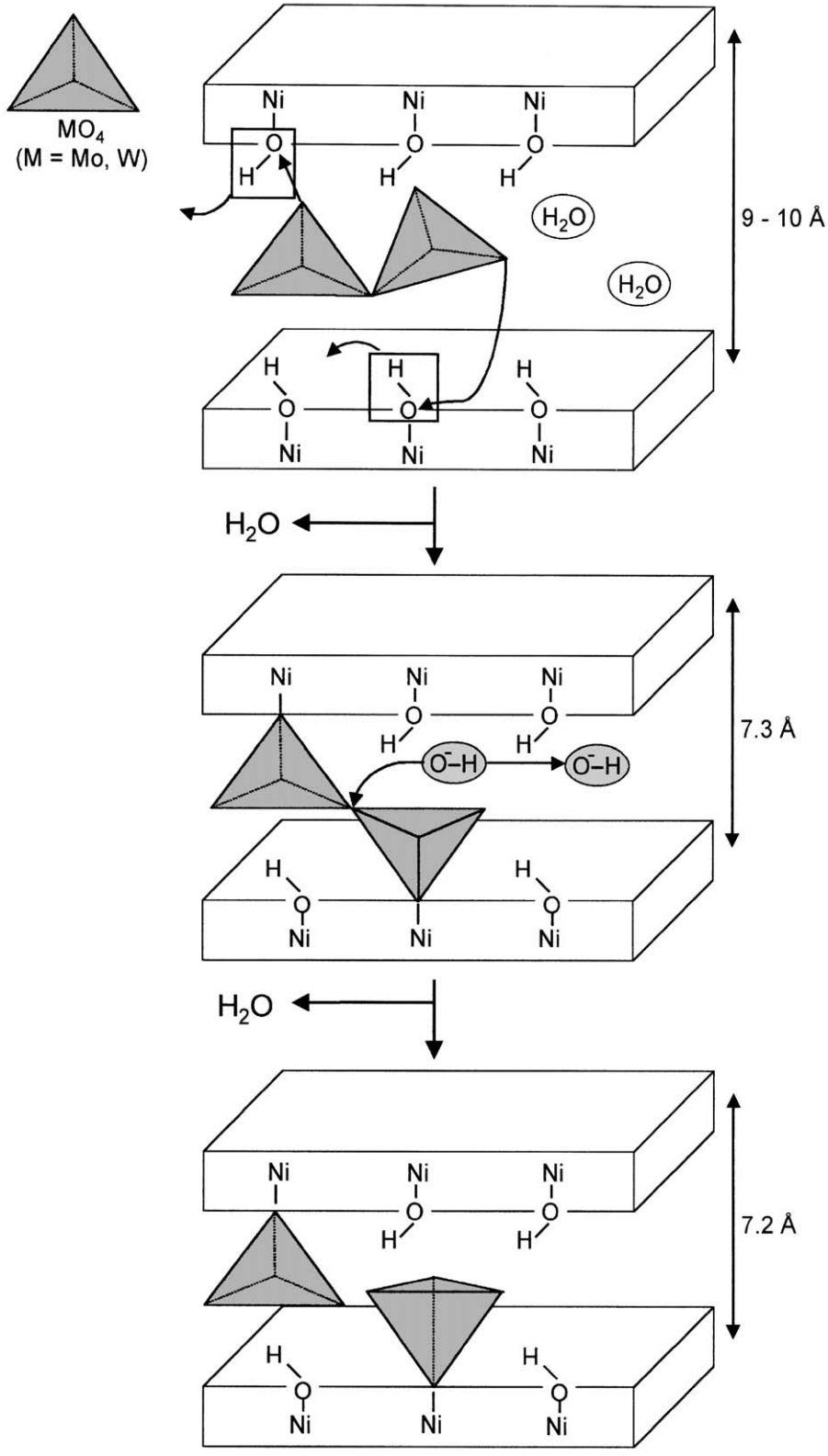

FIG. 12. Schematic representation of the grafting/fragmentation mechanism proposed for the $M_2O_7^{2-}$ (M = Mo, W) entities.

experimental interlamellar distance than the theoretically calculated one.

As a conclusion, the $Mo_2O_7^{2-}$ entities can be grafted to two adjacent slabs, which may exhibit two types of oxygen packing (AB AB) or (AB CA BC). Indeed, the broadness of the XRD lines may be the result of the two grafting hypotheses.

As we have mentioned in a previous part, a change in the evolution of the relative intensity of the first two diffraction peaks (belonging to the (00ℓ) line series) is observed during the thermal treatment (Fig. 1). Indeed, it has been previously shown that the presence of molybdenum or tungsten atoms in a suitable ratio, in the center of the interslab space, induces an inversion of the intensities of the first two diffraction lines, in comparison to $LDH_{0.30}(CO_3)$ (6). This behavior is not observed for the thermally treated materials; in order to understand it, a simulation of the XRD patterns of the thermally treated LDHs was performed with the DIFFaX program (17); only the results for $LDH_{0.30}$(W) are reported here. For the simulation, a centrosymmetric NiO_2 slab was built up by using the $-3\,m$ point symmetry and the following positions for nickel (0, 0, 0) and oxygen atoms (1/3, 2/3, 0.137). The hydrogen atoms were neglected. The overall tungstate entities were considered as generating two tungsten planes, with the positions of W (0, 0, 0), located at a distance of 2.74 Å from the nickel planes, and one oxygen plane, with the positions of O (0, 0, 0), in the center of the interslab space (Fig. 11). The layers were then stacked along the c direction on the basis of an (AB AB) packing oxygen layers. A Gaussian function was used for the profile simulation. Figure 11 presents a scheme of such a configuration as well as the experimental and calculated XRD patterns of both the starting and the thermally treated $LDH_{0.30}$(W) phases. It is clearly shown that there is a good accordance between the experimental XRD pattern and the diagram that was calculated for the 0.30 W:Ni and 0.40 $W:O_{interslab}$ ratios for the thermally treated material. A similar result was observed for the thermally treated $LDH_{0.30}$(Mo) phase. In brief, the change in relative intensity of the (00ℓ) lines is, therefore, correlated to the modification in the arrangement of the interslab $M_2O_7^{2-}$ entities, which is entailed by the thermal treatment.

In the discussion of the TGA results, we have shown that the $M_2O_7^{2-}$ entities are grafted to the slabs in first step, then the loss of water molecules with increasing temperature could be explained by the fragmentation of $M_2O_7^{2-}$ species grafted to the slabs into two separated MO_4 tetrahedra. The following grafting/fragmentation mechanism can be proposed (Fig. 12): in the first step of the thermal treatment, two iono-covalent bonds are formed between two oxygen ions of the intercalated oxoanion and two cations of the slabs. This can be considered as a local anionic exchange, the two hydroxyl groups remaining into the interslab space. At this step, only intercalated water is removed. In a second step, one of the hydroxyl groups reacts with the $M_2O_7^{2-}$ entity, leading to two separated MO_4 entities and a proton. This proton reacts with the second hydroxyl group in order to form a water molecule, which is removed. The mechanism could be resumed as follows:

$$2\,[\text{Slab}] - \text{OH} + M_2O_7^{2-} \rightarrow [\text{Slab}] - M_2O_7 - [\text{Slab}]$$

$$+2\,\text{OH}^- \rightarrow 2[\text{Slab}] - \text{O}MO_3^- + \text{H}_2\text{O}$$

In order to confirm the existence of such fragmented MO_4 entities, which was not unambiguously proved at this time, EXAFS measurements are planned for the materials treated at 300°C.

CONCLUSION

$M_2O_7^{2-}$ oxometalate species intercalated LDHs (M = Mo, W) were studied in the present work. It has been shown that a grafting takes place between the oxoanions and the slabs, which results from strong iono-covalent bonds between the $M_2O_7^{2-}$ entities and the slab hydroxyls. The EXAFS study has allowed to conclude that the grafting of the molybdate entities is performed to two consecutive slabs, with an (AB AB) or an (AB CA BC) oxygen packing. Simulations of the XRD patterns of the thermally treated LDHs have also allowed to address the relative intensites of the first two (00ℓ) lines, which are not inverted, contrary to the starting materials. This is due to the displacement of the molybdenum or tungsten atoms on all sides of the center of the interslab space. Besides, it has been shown that the bi-grafting of the oxometalate species to the slabs creates large pillars, which give a higher thermal stability to the materials, compared to the homologous carbonate-inserted LDH.

ACKNOWLEDGMENTS

The authors thank D. Denux for his technical support, the staff of LURE for its help as well as Région Aquitaine for its financial support.

REFERENCES

1. F. Canavi, F. Trifiro, and A. Vaccari, *Catal. Today* **11,** 173 (1991).
2. A. Vaccari, *Catal. Today* **41,** 53 (1998).
3. V. Rives, and M. A. Ulibarri, *Coord. Chem. Rev.* **181,** 61 (1999).
4. C. Delmas, and Y. Borthomieu, *J. Solid State Chem.* **104,** 345 (1993).

5. K. S. Han, L. Guerlou-Demourgues, and C. Delmas, *Solid State Ionics* **84,** 227 (1996).
6. C. Vaysse, L. Guerlou-Demourgues, A. Demourgues, F. Lazartigues, F. Fertier, and C. Delmas, *J. Mater. Chem.* **12,** 1035 (2002).
7. L. Bigey, C. Depège, A. De Roy, and J. P. Besse, *J. Phys. IV France* (*C2*) **7,** 949 (1997).
8. L. Bigey, F. Malherbe, A. De Roy, and J. P. Besse, *Mol. Cryst. Liq. Cryst.* **311,** 221 (1998).
9. F. Malherbe and J. P. Besse, *J. Solid State Chem.* **155,** 332 (2000).
10. F. Malherbe, L. Bigey, C. Forano, A. De Roy and J. P. Besse, *J. Chem. Soc.: Dalton Trans.* 3831 (1999).
11. A. Mendiboure and R. Schöllhorn, *Rev. Chim. Miner.* **23,** 819 (1986).
12. A. F. Wells, "Structural Inorganic Chemistry." Oxford: Oxford Univ. Press, 1950.
13. E. Kanezaki, *Solid State Ionics* **106**(3–4), 279 (1998).
14. E. Kanezaki, *Inorg. Chem.* **37**(10), 2588 (1998).
15. F. Rey, V. Fornes, and J. M. Rojo, *J. Chem. Soc.: Faraday Trans.* **88**(15), 2233 (1992).
16. C. Vaysse, L. Guerlou-Demourgues, and C. Delmas, *Inorg. Chem.*, submitted (2002).
17. M. Treacy, J. Newsam, and M. Deem, *Proc. R. Soc. London Ser. A* **43,** 499 (1991).